J. Chem. Thermodynamics 1976, 8, 583–600

Thermodynamics of Fe(II)Fe(III) oxide systems
II. Zinc- and cadmium-doped Fe_3O_4 and crystalline magnetite [a]

JAMES J. BARTEL[b] and EDGAR F. WESTRUM, JR.[c]

Department of Chemistry, The University of Michigan, Ann Arbor, Michigan 48104, U.S.A.

(*Received 16 October 1975*)

Four doped samples of composition $M_xFe_{3-x}O_4$, in which for M = cadmium, $x = 0.005$ and 0.010, and for M = zinc, $x = 0.005$ and 0.066, were prepared using a high-temperature solid-state ceramic technique. X-ray, magneto-t.g.a., chemical analysis, and comparative thermophysical data confirmed the quality of the samples. The heat capacities of the doped samples were measured from 5 to 350 K using adiabatic calorimetry; magnetite crystals were studied over the range 65 to 350 K by the same technique. Temperature elevation of the higher-temperature transition was observed for the doped sample $Zn_{0.005}Fe_{2.995}O_4$. Elimination of the double anomaly is occasioned by high mole fraction of dopant and crystal-structure expansion as demonstrated by the doped samples $Cd_{0.005}Fe_{2.995}O_4$, $Cd_{0.010}Fe_{2.990}O_4$, and $Zn_{0.066}Fe_{2.934}O_4$. Displacements of the lower-temperature transition to higher and lower temperatures were observed. Systematic variations in the transitional thermal properties have been related also to dopant type and mole fraction. Tentative assignment of the two lambda-type transitions to interdependent Wigner and structural order-disorder mechanisms is proposed. Although adjuvant measurements would be desirable to confirm this analysis, the pre-eminence of the heat capacity as a sensitive detector and indicator of dopant level has been demonstrated.

1. Introduction

Parks and Kelly[1] observed a transition over the temperature interval 113 to 117 K from low-temperature heat-capacity measurements of magnetite crystals by drop calorimetry over the range 90 to 295 K. Millar[2] made heat-capacity measurements on a magnetite single crystal containing 99.0 moles per cent Fe_3O_4 and found a single heat-capacity anomaly at 114.2 K. Westrum and Grønvold[3] subsequently revealed the presence of a bifurcated anomaly with the heat-capacity maxima at 113.3 and 118.88 K by adiabatic calorimetric measurements from 5 to 350 K. Confirmation of the bifurcated anomaly was reported by the present authors[4] and the

[a] Supported by the National Science Foundation. Based on a dissertation submitted to the Horace H. Rackham School of Graduate Studies at the University of Michigan in partial fulfillment of the requirements for the Ph.D. degree by J.J.B. Paper I in this series immediately precedes this paper.

[b] Present address: Sandia Laboratories, Division 8313, Livermore, Calif., 94550, U.S.A.

[c] To whom correspondence concerning this paper should be directed.

thermodynamic measurements of this hydrothermally prepared material are detailed elsewhere.[5]

The paucity of other physical measurements extending through the transition region at closely spaced temperatures and the general confusion, despite great current interest in metal-insulator transitions, about the mechanism of the so-called Verwey transition in Fe_3O_4, encouraged us to undertake further heat-capacity studies with deliberately selected transition-metal ions introduced on to particular sites of the inverse spinel lattice of Fe_3O_4.

Although resistivity changes observed in Fe_3O_4 have been interpreted variously, regardless of mechanism, the electronic transformations are considered to involve primarily the octahedral B-sites.[6–8] Certain A-site dopant ions effectively diminish Fe^{2+} on the B-sites without contributing conduction electrons; certain other A-site ions increase the size of the cubic sub-cell as well as reduce electron concentration on the B-sites. Since the Shannon-Prewitt[9] (S-P) radii for A-site ions listed in table 1 for Zn^{2+} and Fe^{3+} are quite close (as are their spinel lattice parameters), the effect

TABLE 1. 4-Coordinate Shannon-Prewitt radii r_{S-P} for certain ions favoring A-site substitution and spinel a_0 parameters for MFe_2O_4

Ion M	r_{S-P}/nm [a]	a_0/nm
Fe^{3+}	0.063	0.8396 [b]
Zn^{2+}	0.050	0.8445 [c]
Cd^{2+}	0.095	0.869 [d]
Mn^{2+}	0.081	

[a] Reference 9. [b] Reference 10. [c] Reference 11. [d] Reference 12.

of zinc doping decreases the Fe^{2+} B-site mole fractions in accordance with the formula:

$$(M_x^{2+}Fe_{1-x}^{3+})[Fe_{1-x}^{2+}Fe_{1+x}^{3+}O_4], \quad (1)$$

in which parentheses ( ) refer to the tetrahedral A-sites and brackets [ ] to the octahedral B-sites, and M to the dopant ion. Since Cd^{2+} has a much larger S-P radius, its presence decreases the B-site electron concentration while increasing the sub-cell size. In addition, Zn^{2+} and Cd^{2+} meet the following criteria deemed essential to minimize the perturbations in the system: (1) specific A-site preference, (2) well-defined oxidation state, and (3) completely filled d-orbitals. It will be noted that (1) eliminates the possibility of entropy contributions from randomization of the dopant ion over the A and B sites; whereas (2) and (3) eliminate the possibility of the dopant contribution of conduction electrons and the minimization of double-exchange interactions, respectively.

We report in this paper results of adiabatic heat-capacity determinations for synthetic samples of Fe_3O_4 doped with $x = 0.010$ and 0.005 for M = cadmium and with $x = 0.066$ and 0.005 for M = zinc; M and x are defined by formula (1). The availability of two presumably high-purity crystals[13] allowed the study of naturally

doped magnetite also. Because we were concerned about possible subtle effects on both heat capacity and entropy at regions remote from the transition, we examined the thermophysical properties across the entire cryogenic region.

2. Experimental

SAMPLES

Quantities of Johnson-Matthey Grade I "Specpure" (99.998 moles per cent pure with respect to both cations and anions) Fe_2O_3, Fe, and dopant oxide MO, consistent with the reaction:

$$xMO + \tfrac{1}{3}(1-x)Fe + \tfrac{1}{3}(4-x)Fe_2O_3 = M_xFe_{(3-x)}O_4,$$

were dry-mixed in an agate mortar, loaded into a quartz ampoule which was then evacuated to 10^{-6} Torr, and sealed off.† The ampoule and contents were fired at 1070 K for 8 to 14 h; then the furnace was cooled to room temperature. After grinding and sizing (to 200 mesh or less), the sample was compressed in a steel die; the resulting pellet was loaded into a special quartz ampoule packed with alumina wool to prevent movement of the pellet, and the end of the ampoule was fused shut. The then evacuated and sealed ampoule and contents were fired at 1258 K for 24 h and furnace-cooled. Surface layers were removed and the pellet was crushed.

SAMPLE CHARACTERIZATION

Crystallographic analyses of the powdered samples were achieved with a 114.6 mm radius Haegg-type focussing X-ray diffraction camera using $CaK\alpha_1$, radiation (λ = 0.154051 nm) on doped Fe_3O_4 samples ground in an agate mortar with high-purity silicon (a_0 = 0.543062 nm).[14] Exposures of 3.5 h on double-emulsion film (with the front emulsion surface removed during development) minimized the effect of iron fluorescence and yielded good quality patterns. The observed sample 2θ values were adjusted via interpolation of the observed silicon 2θ values referred to accepted values for silicon.[15] Diffraction results were reduced with the least-squares regression program of Lindqvist and Wengelin.[16] Lattice parameters for the doped Fe_3O_4 samples are listed in table 2. A uniform variation of a_0 with mole fraction of dopant would be expected. An expanded Vegard plot, figure 1, shows this behavior

TABLE 2. Lattice parameters for doped Fe_3O_4 samples

Sample	a_0/nm	Sample	a_0/nm
Fe_3O_4	0.83963 [a]	Fe_3O_4	0.83963 [a]
$Zn_{0.005}Fe_{2.995}O_4$	0.83977±0.00014	$Cd_{0.005}Fe_{2.995}O_4$	0.83977±0.00013
$Zn_{0.066}Fe_{2.934}O_4$	0.84005±0.00009 [b]	$Cd_{0.010}Fe_{2.990}O_4$	0.83995±0.00012
$ZnFe_2O_4$	0.84450±0.00006	$Cd_{0.033}Fe_{2.967}O_4$	0.84062±0.00022 [c]
		$CdFe_2O_4$	0.869

[a] Reference 10. [b] Reference 11. [c] Reference 12.

† Throughout this paper Torr = (101.325/760) kPa; cal_{th} = 4.184 J.

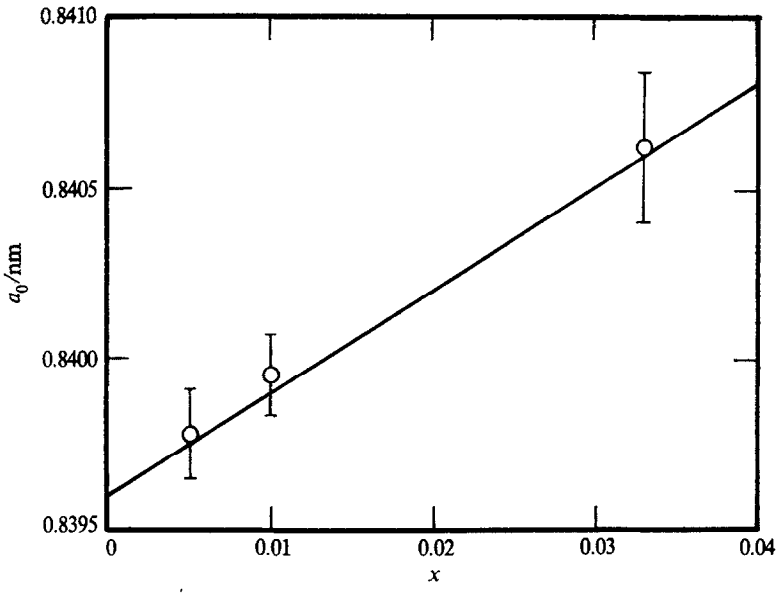

FIGURE 1. Vegard plot for Cd-doped Fe_3O_4: $Cd_xFe_{3-x}O_4$.

for the cadmium-doped materials. The small range in a_0 values between zinc ferrite and Fe_3O_4 precludes use of such a plot, as the experimental imprecision in determination of the parameters exceeds the expected a_0 variation. The general trend of mean a_0 values listed in table 2 is consistent with increasing mole fraction of Zn.

Schwarzkopf Microanalytical Laboratory performed the chemical analysis on samples dissolved in 6 mol dm^{-3} aqueous HCl. Zn and Cd were determined by atomic absorption with a stated probable error of ± 0.02 mole per cent. Fe was determined by dichromate titration to ± 0.03 mole per cent. The results are listed in table 3. Complete X-ray experimental results are available elsewhere.[17]

Néel-point determinations with a Perkin Elmer TSG-1 thermobalance (also listed in table 3) were made in flowing high-purity oxygen-gettered nitrogen or argon gas environments with 20 to 40 mg samples and a heating rate of 10 K min^{-1}. The balance bottle was purged for 2 h before initiating the temperature scan. After observing the zero-field sample mass, the field magnet was placed in position and the temperature scan started. Apparent mass indicated by the balance was the sum of the sample mass and the magnetic attraction between the sample and field magnet. After the magnetic disordering range was traversed, the scan was reversed and the sample returned to 300 K. These magneto-t.g.a. determinations of the ferrimagnetic disordering temperatures and ranges indicated that both were subject to minor systematic variation due to dopant type and mole fraction. No hysteresis was expected or found. Frequent mass-calibration checks of the electrobalance were made. The temperature programmer was calibrated at regular intervals between 373 and 1200 K against five magnetic standards. Temperatures are believed reliable to ± 5 K and the probable error is within ± 2 K.

TABLE 3. Compositions in mass per cent and Néel temperatures of doped-Fe_3O_4 samples

Mode	Zinc	Cadmium	Iron	Oxygen	T(Néel)/K [a]	T_1/K [b]	T_2/K [b]
			Pure Fe_2O_3				
					868	856	888
			$Zn_{0.005}Fe_{2.995}O_4$				
by synthesis	0.141	—	72.162	27.697	853	833	877
by analysis	0.1_3	—	73.4_1	25.9_2			
			$Zn_{0.066}Fe_{2.934}O_4$				
by synthesis	1.877	—	70.567	27.556			
by analysis	1.89	—	71.2_1	—	833	788	868
	1.7_7	—	79.9_7	—			
			$Cd_{0.005}Fe_{2.995}O_4$				
by synthesis	—	0.232	72.13	27.62	851	837	878
by analysis	—	0.2_5	72.9_4	26.8_0			
			$Cd_{0.010}Fe_{2.990}O_4$				
by synthesis	—	0.566	71.561	27.561	852	824	885
by analysis	—	0.5_9	73.4_1	25.9_4			

[a] Taken at maximum change of slope of the curve of apparent mass against temperature from the magneto-t.g.a.

[b] From start (T_1) to completion (T_2) of magnetic disordering.

CALORIMETRY

Low-temperature heat-capacity measurements of magnetite crystals were made in the Mark-III adiabatic cryostat over the range 65 to 350 K. Details of the cryostat construction and calibration of the measuring circuits are described by Carlson.[18] The Mark-II adiabatic cryostat[19] was used in measuring the heat capacity of the doped Fe_3O_4 samples over the temperature range 5 to 350 K. Sample calorimeters are gold-plated thin-walled copper containers with axial re-entrant wells for the thermometer + heater assembly. Thin radial vanes within the calorimeter aid thermal equilibration of calorimeter and contents. Capsule-type platinum-resistance thermometers, calibrated by the National Bureau of Standards (N.B.S.) were used.

TABLE 4. Calorimeter and sample information: V denotes the internal volume of the calorimeter, m the sample mass, M the molar mass, and p(He) the pressure of helium added to improve thermal contact and equilibration between sample and calorimeter

(Torr = (101.325/760) kPa)

Sample	Calorimeter	V/cm^3	m/g	M/g mol^{-1} [a]	p(He)/Torr
Magnetite crystals	W-42	93.00	212.4474	231.539	70.0
$Zn_{0.066}Fe_{2.934}O_4$	W-52	59.11	63.6988	232.121	57.5
$Cd_{0.010}Fe_{2.990}O_4$	W-52	59.11	43.1836	232.113	76.0
$Zn_{0.005}Fe_{2.995}O_4$	W-52	59.11	70.2275	231.586	57.0
$Cd_{0.005}Fe_{2.995}O_4$	W-52	59.11	77.6872	231.821	42.0

[a] Accurate to two decimal places; IUPAC Commission on Atomic Weights 1972.

Calibration is referred to the "International Practical Temperature Scale of 1948, Text Revision of 1960" as adopted in 1960,[20] defined between 190.18 K and 903.65 K. From 10 to 90 K, the N.B.S. 1955 provisional scale was used and below 10 K a provisional scale was adopted. Relevant calorimeter and sample information and molar masses used to calculate molar heat capacities from observed values are given in table 4 for the various samples.

After establishing the temperature of transition within 2 K, transition regions were detailed by several series of determinations, usually at 0.5 K increments. Carefully selected temperature at the start of a series enabled determination of the transitional heat capacity maxima to within ± 0.01 K. Individual enthalpy determinations were bracketed by short energy inputs before and after enthalpy determinations. End-point adjustments were made to enthalpy determinations for uniformity. No disagreements were noted between enthalpies obtained *via* summation of small incremental determinations of heat capacity through the transition and single energy inputs through the entire transition region. The measured heat capacities were corrected for the heat capacity of the empty calorimeter, which was measured in a separate series of experiments. Slight adjustments were made for differences in the amount of gaseous helium used with the calorimeter when it was run empty and when it was run with the various Fe_3O_4 samples.

3. Results

HEAT CAPACITIES

Portions of experimentally determined heat capacities for the several samples as a function of temperature are shown in figure 2 and values for the individual determinations are presented in tables 5 to 9 in chronological order so that temperature increments across individual runs in a series may be estimated from adjacent mean temperatures. An analytically determined curvature correction has been applied to the measured values of $\Delta H/\Delta T$ in non-transitional regions. These results are considered to be characterized by a probable error of about 5 per cent near 10 K, decreasing to 0.8 per cent at 20 K, and to less than 0.2 per cent above 30 K. The determinations of the enthalpies and entropies of transition are presented in table 10.

Magnetite crystals. As shown in figure 2(b), the heat capacity of this sample displayed a large sharp anomaly with a high-temperature shoulder. It contrasts with the results for Millar's sample[2] on the same figure as well as with the transition regions of pure- and hydrothermal-Fe_3O_4 samples[3, 5] described elsewhere. Several series of measurements were performed to define clearly the form of the shoulder. Heat-capacity results are presented in table 5. The transition temperature upon cooling was observed to be the same as that upon heating. The heat capacity of the empty calorimeter used for the magnetite crystals was determined in the Mark-II cryostat, not Mark-III. Expected differences of observed heat capacity are believed to be less than the experimental precision, ± 0.03 per cent.

$x(\mathrm{Zn}) = 0.005$. Two well separated anomalies were observed in the heat capacity of this sample and are shown in figure 3. Differences in the heat capacity of this sample

TABLE 5. Experimental heat capacity of magnetite crystals
($cal_{th} = 4.184$ J)

T/K	C_p/$cal_{th}\,K^{-1}\,mol^{-1}$	T/K	C_p/$cal_{th}\,K^{-1}\,mol^{-1}$	T/K	C_p/$cal_{th}\,K^{-1}\,mol^{-1}$	T/K	C_p/$cal_{th}\,K^{-1}\,mol^{-1}$
Series I		113.07	17.04	121.64	19.56	342.91	39.38
63.86	5.787	113.63	17.46	122.40	18.99	347.25	39.68
70.96	7.074	114.70	18.72	127.39	18.72		
77.10	8.256	115.20	20.66			Series XIII	
82.59	9.375			Series IX		112.20	16.94
		Series VI		190.36	27.05	Enthalpy detn. B	
Series II		109.71	15.61	199.56	27.95	127.98	18.76
82.76	9.407	111.18	16.47	208.55	28.90		
87.79	10.495	112.32	16.95	217.31	29.85	Series XIV	
92.46	11.381	113.02	17.21	225.87	30.71	115.80	31.07
96.86	12.339	113.71	18.27	234.25	31.52	116.45	46.89
101.02	13.147	114.52	(18.10)	194.51	27.41	116.92	63.06
		115.28	20.10	203.55	28.39	117.06	73.08
Series III		115.91	30.46	212.37	29.34	117.15	84.75
100.01	12.945	116.40	45.80	220.97	30.27	117.23	96.85
102.27	13.250	116.86	61.12	229.41	30.94	117.31	106.15
102.87	13.486	117.15	91.32	237.67	31.89	117.48	86.63
103.83	13.738	117.37	109.60	245.77	32.56	117.54	76.08
104.78	13.940	117.62	70.45	253.75	33.22	117.61	66.23
105.72	14.128	118.02	37.20	261.62	33.87	117.69	56.50
106.64	14.391	118.56	30.90	269.36	34.45	117.84	45.64
107.56	14.603	119.14	29.07	272.34	34.71	119.13	29.39
108.46	14.955	119.75	27.11	272.83	34.84	121.80	19.92
		120.55	22.20	273.32	34.87	124.85	18.56
Series IV		121.33	19.92	273.80	34.46	127.94	18.80
110.23	15.96					139.11	20.31
111.08	16.42	Series VII		Series XI		145.28	21.36
111.92	16.83	113.17	17.57	272.88	34.70	151.25	22.08
112.75	17.14	Enthalpy detn. A		273.53	34.88	157.07	22.90
113.57	17.58	125.69	18.63	274.17	35.04	162.73	23.66
114.38	18.40			274.81	35.06	168.64	24.34
		Series VIII		277.87	35.14		
Series V		113.44	17.46	283.34	35.56	Series XV	
100.01	12.925	114.51	18.72	288.76	35.74	137.19	20.28
101.63	13.267	115.67	28.45	294.14	36.32	143.49	21.07
103.22	13.613	116.51	48.85	299.48	36.68	149.61	21.80
104.86	13.946	117.06	81.91			155.56	22.70
106.41	14.305	117.47	95.86	Series XII		161.35	23.49
107.64	14.634	117.80	44.26	294.08	36.27	166.99	24.22
108.55	14.979	118.13	33.66	300.03	36.79	172.51	24.88
109.49	15.49	118.49	32.49	306.59	37.05	177.92	25.15
110.21	15.95	118.86	29.09	312.44	37.54	183.22	26.14
110.82	16.24	119.26	28.80	317.60	37.86	188.44	26.77
111.40	16.58	119.66	27.23	322.73	38.27		
111.96	16.81	120.08	25.40	327.82	38.41	Series XVI	
112.52	17.03	120.53	22.33	332.88	38.80	110.68	16.14
		121.01	20.54	337.91	39.10	Enthalpy detn. C	

TABLE 6. Experimental heat capacity of Zn-doped Fe_3O_4: $Zn_{0.005}Fe_{2.995}O_4$ ($cal_{th} = 4.184$ J)

T/K	C_p/$cal_{th}\,K^{-1}\,mol^{-1}$	T/K	C_p/$cal_{th}\,K^{-1}\,mol^{-1}$	T/K	C_p/$cal_{th}\,K^{-1}\,mol^{-1}$	T/K	C_p/$cal_{th}\,K^{-1}\,mol^{-1}$
Series I		106.93	15.04	218.21	29.80	15.84	0.123
86.99	10.446	107.85	15.66	228.36	30.67	17.33	0.155
92.64	11.611	108.67	20.37	238.28	31.56	18.91	0.208
97.86	12.772	109.33	31.15	248.00	32.39	20.70	0.279
102.73	13.873	109.91	44.00	257.52	33.16	22.82	0.387
107.15	16.68	110.39	52.09	267.07	33.90	25.00	0.524
110.16	46.53	110.75	52.98	276.63	34.64	27.22	0.683
112.68	24.33	111.12	46.38	286.05	35.31	30.05	0.940
115.99	20.91	111.43	39.48	295.32	35.95	33.53	1.300
119.36	22.82	111.85	26.18	304.68	36.58	37.41	1.763
122.90	19.98	112.53	20.88			41.82	2.338
126.67	18.51	114.37	20.83	Series VI		46.50	3.022
132.71	19.42			294.29	35.91	51.61	3.831
140.86	20.62	Series IV		303.91	36.52	57.37	4.791
		116.14	20.72	313.39	37.12	62.92	5.778
Series II		116.88	20.85	322.76	37.62	68.24	6.698
90.87	11.235	117.43	20.47	332.00	38.17		
100.09	13.229	117.80	20.69			Series IX	
105.36	14.582	118.16	21.64	Series VII		100.87	13.462
108.67	21.80	118.50	24.37	56.67	4.672	Enthalpy detn. C	
109.69	38.83	118.80	30.35	63.77	5.930	128.75	18.81
110.16	48.74	119.06	36.14	70.54	7.156		
110.57	53.73	119.32	29.83	77.96	8.583	Series X	
110.97	48.76	119.65	20.01	85.16	10.055	117.81	19.67
111.46	34.86	120.04	17.95	91.56	11.377	118.14	21.21
112.31	23.23	120.65	17.80	98.79	12.966	118.45	23.66
113.30	20.45	121.66	17.84	Enthalpy detn. B		118.69	28.39
114.13	20.58	126.61	18.53	131.22	19.19	118.83	31.05
114.96	20.97	135.09	19.78			118.97	34.14
115.77	21.19	143.14	20.94	Series VIII		119.09	36.10
116.59	20.93	151.21	22.07	4.84	0.006	119.22	32.48
117.41	20.55	159.73	23.17	5.85	0.009	119.37	26.16
118.37	24.39	168.02	24.23	6.64	0.006	119.54	21.07
119.22	31.58	176.34	25.22	7.39	0.010	119.73	18.62
119.96	18.43			8.17	0.024	120.03	17.89
120.86	17.74	Series V		8.96	0.034	120.75	17.79
121.99	17.82	171.49	24.65	9.62	0.040		
		180.69	25.73	10.36	0.058		
Series III		190.27	26.83	11.48	0.066		
99.77	13.203	199.57	27.84	12.87	0.075		
106.00	14.739	208.62	28.80	14.37	0.096		

TABLE 7. Experimental heat capacity of Zn-doped Fe_3O_4: $Zn_{0.066}Fe_{2.934}O_4$ ($cal_{th} = 4.184$ J)

T/K	C_p/$cal_{th}\,K^{-1}\,mol^{-1}$	T/K	C_p/$cal_{th}\,K^{-1}\,mol^{-1}$	T/K	C_p/$cal_{th}\,K^{-1}\,mol^{-1}$	T/K	C_p/$cal_{th}\,K^{-1}\,mol^{-1}$
Series I		229.58	31.09	9.64	0.050	13.50	0.092
93.54	12.780	239.42	31.98	10.39	0.065	14.85	0.111
99.67	13.901	249.32	32.81	11.58	0.074	16.22	0.136
105.42	14.945	259.28	33.59	12.85	0.089	17.65	0.177
110.84	15.93	269.33	34.36	14.27	0.112	19.22	0.225
116.01	16.85	279.47	35.09	15.88	0.144	21.08	0.309
120.96	17.71	289.62	35.81	17.53	0.190	23.19	0.419
125.72	18.51	299.87	36.51	19.21	0.252	25.49	0.572
130.31	19.27	309.98	37.13	21.06	0.339	27.92	0.756
134.78	19.96	319.96	37.70	23.13	0.456	30.78	1.031
140.04	20.78	329.82	38.25	25.35	0.612	34.48	1.437
146.05	21.65	339.58	38.84	27.66	0.806	38.86	1.977
Series II		347.30	39.34	30.07	1.037	43.49	2.616
82.08	10.581	Series IV		32.69	1.328	48.01	3.301
89.22	12.004	60.94	6.122	35.48	1.672	52.88	4.077
95.71	13.194	67.17	7.435	38.46	2.073	57.81	4.925
106.27	15.14	71.75	8.420	41.91	2.578	76.13	8.483
120.28	17.62	75.90	9.292	45.88	3.216	Series VII	
132.86	19.69	79.74	10.088	50.24	4.000	88.09	11.025
144.49	21.44	83.89	10.944	54.39	4.763	Enthalpy detn. A	
155.39	22.98	88.35	11.816	58.69	5.626	116.73	16.87
165.78	24.34	93.03	12.697	Series VI		Series IX	
Series III		Series V		4.50	(0.021)	86.70	10.710
149.93	22.24	4.73	0.014	5.49	0.002	Enthalpy detn. B	
160.23	23.62	5.30	0.008	6.57	0.005	115.50	16.70
170.09	24.85	5.74	0.005	7.18	0.004	Series X	
179.58	25.99	6.38	0.009	8.00	0.011	86.69	10.704
189.25	27.10	7.10	0.012	8.67	0.015	Enthalpy detn. C	
199.13	28.15	7.74	0.017	9.32	0.033	115.60	16.70
209.22	29.21	8.42	0.031	10.17	0.054		
219.52	30.19	9.10	0.042	11.07	0.058		
				12.21	0.070		

TABLE 8. Experimental heat capacity of Cd-doped Fe_3O_4: $Cd_{0.005}Fe_{2.995}O_4$
(cal_{th} = 4.184 J)

T/K	C_p/$cal_{th}\,K^{-1}\,mol^{-1}$	T/K	C_p/$cal_{th}\,K^{-1}\,mol^{-1}$	T/K	C_p/$cal_{th}\,K^{-1}\,mol^{-1}$	T/K	C_p/$cal_{th}\,K^{-1}\,mol^{-1}$
Series II		6.00	0.009	62.99	5.788	190.51	26.89
89.61	10.945	6.33	0.015	68.68	6.820	200.56	27.98
94.22	11.878	7.41	0.018	75.15	8.025	210.72	29.06
98.53	12.809	8.07	0.020	79.59	8.904	221.07	30.03
102.61	13.691	8.73	0.025	83.51	9.696	231.40	30.95
106.47	14.620	9.47	0.030	89.83	10.983	241.49	31.83
109.69	15.85	10.39	0.053	96.20	12.298	251.37	32.66
111.71	22.19	11.59	0.057	102.93	13.779	261.01	33.49
112.88	36.03	12.98	0.074	Enthalpy detn. A		270.53	34.21
113.56	45.19	14.36	0.099	119.30	17.51	280.09	34.86
113.92	53.87	15.86	0.121			289.68	35.76
114.22	67.28	17.41	0.161	Series IV		299.40	36.24
114.47	88.27	19.08	0.208	90.46	11.101	309.55	36.82
114.66	101.49	20.96	0.292	98.64	12.819	319.89	37.48
114.87	82.50	23.08	0.403	104.63	14.174	330.10	38.08
115.18	45.99	25.46	0.555	Enthalpy detn. B		340.20	38.69
115.71	22.55	28.24	0.776	119.88	17.55	347.21	39.06
116.46	17.66	31.58	1.095	126.44	18.53		
117.69	17.40	35.37	1.519	134.42	19.88		
119.33	17.46	39.39	2.018	143.93	21.10		
		43.56	2.593	152.52	22.28		
Series III		47.88	3.420	161.65	23.47		
		52.33	3.949	171.02	24.65		
5.30	0.013	57.36	4.793	180.60	25.78		

TABLE 9. Experimental heat capacity of Cd-doped Fe_3O_4: $Cd_{0.010}Fe_{2.990}O_4$ (cal_{th} = 4.184 J)

T/K	C_p/cal_{th} K^{-1} mol^{-1}	T/K	C_p/cal_{th} K^{-1} mol^{-1}	T/K	C_p/cal_{th} K^{-1} mol^{-1}	T/K	C_p/cal_{th} K^{-1} mol^{-1}
Series I		103.86	23.62	257.13	33.20	105.19	20.09
54.71	4.395	104.93	29.38	266.67	33.91	105.38	29.70
63.20	5.911	105.43	31.09			105.53	29.74
70.50	7.250	105.91	31.44	Series IV		105.68	29.04
75.84	8.288	106.39	30.51	250.17	32.64	105.82	29.96
80.67	9.305	107.41	25.66	259.80	33.41	105.97	29.35
85.11	10.312	109.15	18.32	269.60	34.18	106.12	28.94
89.25	11.273	111.11	16.29	279.24	34.91	107.40	25.37
93.13	12.236	113.13	16.34	288.75	35.55	110.12	16.95
96.79	13.289			298.45	36.23	113.17	16.33
100.20	15.19	Series III		308.33	36.84		
103.16	21.64	140.81	20.68	318.10	37.47	Series VI	
105.18	30.52	151.36	22.17	327.75	38.07	97.54	13.721
106.60	29.78	164.27	23.92	337.32	38.57	102.71	20.82
108.18	21.54	176.70	25.40	343.97	38.89	105.22	29.89
110.05	16.89	185.87	26.45	347.74	39.15	105.70	31.11
112.56	16.30	195.88	27.56			106.18	30.72
115.56	16.67	206.70	28.67	Series V		106.80	28.54
		217.23	29.75	95.53	12.952	108.03	21.97
Series II		227.51	30.68	101.92	17.94	110.41	16.71
98.87	14.372	237.57	31.57	103.84	23.90	112.93	16.31
102.63	19.44	247.44	32.43	104.68	28.25		

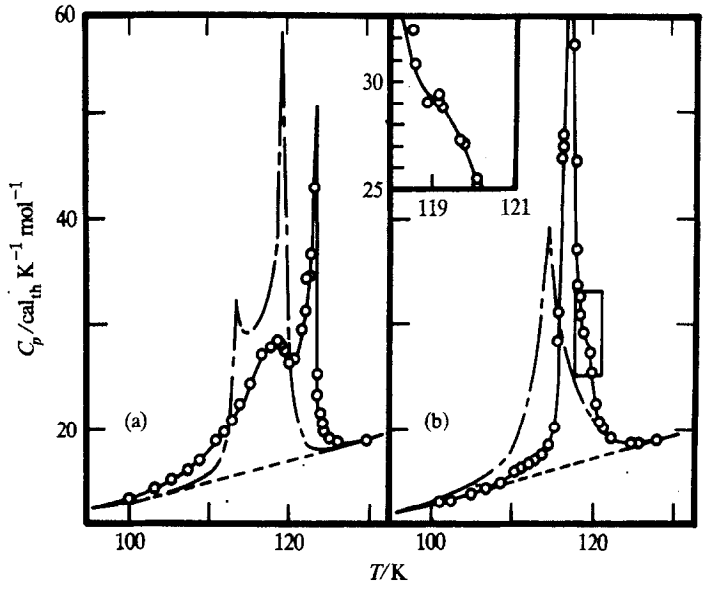

FIGURE 2. Heat capacities in the transition regions of a, — · —, Fe_3O_4,[3] and —○—, hydrothermal magnetite;[12] b, — · —, Millar magnetite,[2] and —○—magnetite crystals.

and of pure Fe_3O_4 are shown in figures 4 and 5. Heat capacities will be found in table 6. Enthalpies and entropies of transition are presented in table 10.

$x(Zn) = 0.066$. No obvious anomalies were found in this sample. Figures 3, 4, and 5 also display the deviations of the heat capacity of this as well as of the other doped Fe_3O_4 samples. ΔC_p is the difference between the heat capacities of the doped Fe_3O_4

TABLE 10. Enthalpy and entropy of transition
($cal_{th} = 4.184$ J)

Enthalpy detn.	T_1 / K	T_2 / K	$H(T_2)-H(T_1)$ / $cal_{th}\ mol^{-1}$	$H(126\ K)-H(109\ K)$ / $cal_{th}\ mol^{-1}$
		Magnetite crystals		
Series VII	113.65	125.90	353.0	427.3
Series XIII	113.88	126.46	359.5	431.2
Series XVIII	111.12	124.07	362.1	430.1
				Mean: 429.5±1.5
				Lattice: 289
		$\Delta H_t = 140\ cal_{th}\ mol^{-1}$	$\Delta S_t = 1.22\ cal_{th}\ K^{-1}\ mol^{-1}$	
		$Zn_{0.005}Fe_{2.995}O_4$		$H(164\ K)-H(99\ K)$ / $cal_{th}\ mol^{-1}$
Series I	100.37	124.81	515.31	1358.8
Series VII	102.98	128.25	542.91	1358.2
Series IX	104.07	125.76	481.78	1358.2
				Mean: 1358.4±0.3
				Lattice: 1216
		$\Delta H_t = 142\ cal_{th}\ mol^{-1}$	$\Delta S_t = 1.20\ cal_{th}\ K^{-1}\ mol^{-1}$	
		$Cd_{0.010}Fe_{2.990}O_4$		$H(85\ K)-H(137\ K)$ / $cal_{th}\ mol^{-1}$
Series VII	84.44	119.30	569.4	894.4
Series IX	83.09	118.10	562.5	894.3
Series X	82.92	118.22	566.3	894.5
				Mean: 894.4±0.1
				Lattice: 790
		$\Delta H_t = 104\ cal_{th}\ mol^{-1}$	$\Delta S_t = 0.95\ cal_{th}\ K^{-1}\ mol^{-1}$	
		$Cd_{0.005}Fe_{2.995}O_4$		$H(160\ K)-H(100\ K)$ / $cal_{th}\ mol^{-1}$
Series II	100.62	124.15	436.058	1263.2
Series III	106.52	121.20	372.951	1263.4
Series IV	106.76	121.82	381.223	1264.2
				Mean: 1263.6±0.6
				Lattice: 1109
		$\Delta H_t = 155\ cal_{th}\ mol^{-1}$	$\Delta S_t = 1.34\ cal_{th}\ K^{-1}\ mol^{-1}$	

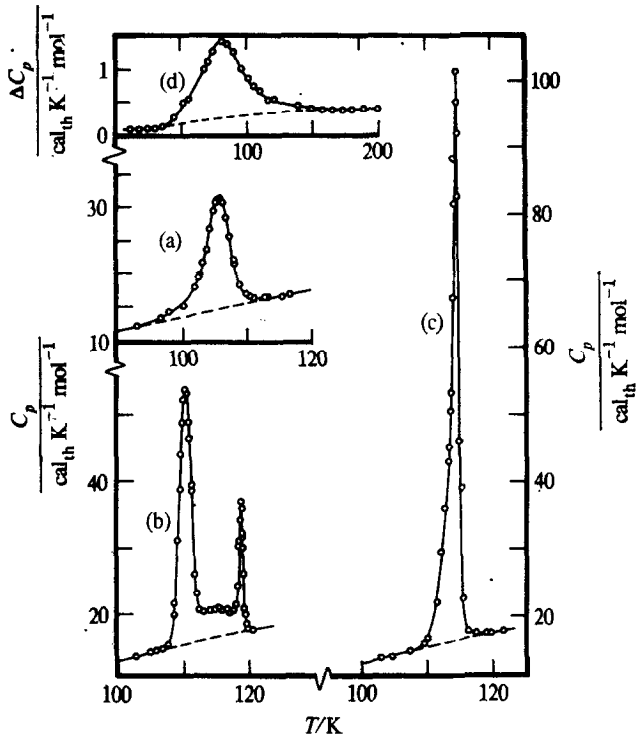

FIGURE 3. Heat capacity C_p in the transition region of a, $Cd_{0.010}Fe_{2.990}O_4$; b, $Zn_{0.005}Fe_{2.995}O_4$; c, $Cd_{0.005}Fe_{2.995}O_4$; and d, $\Delta C_p = \{C_p(\text{sample}) - C_p(\text{lattice})$ for $Zn_{0.066}Fe_{2.934}O_4$.

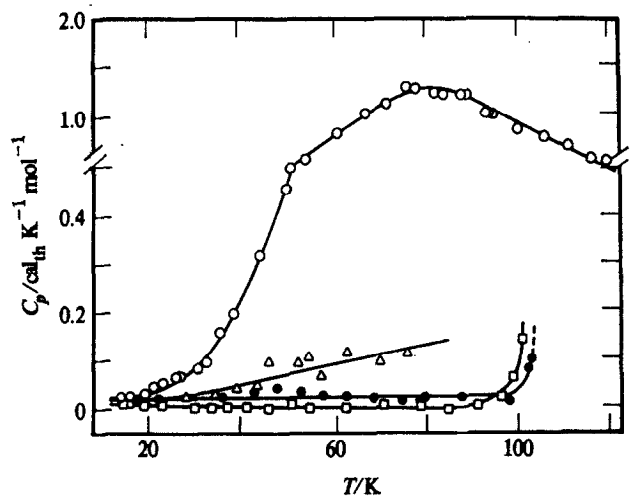

FIGURE 4. Heat capacity increments relative to pure Fe_3O_4 for several samples below the Verwey transition. △, $Cd_{0.010}Fe_{2.990}O_4$; □, $Zn_{0.005}Fe_{2.995}O_4$; ●, $Cd_{0.005}Fe_{2.995}O_4$; ○, $Zn_{0.066}Fe_{2.934}O_4$. (Note the change of scale at 0.5 cal$_{th}$ K^{-1} mol^{-1}.)

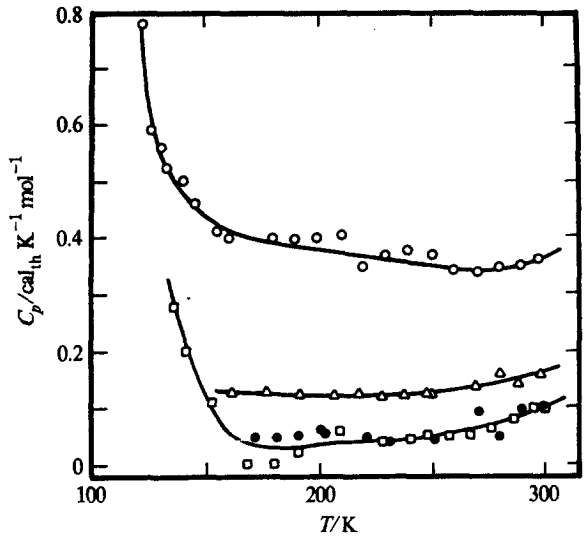

FIGURE 5. Heat-capacity increments relative to pure Fe_3O_4 for several samples above the Verwey transition. △, $Cd_{0.010}Fe_{2.990}O_4$; □, $Zn_{0.005}Fe_{2.995}O_4$; ●, $Cd_{0.005}Fe_{2.995}O_4$; ○, $Zn_{0.066}Fe_{2.934}O_4$.

samples and pure Fe_3O_4. For $x(Zn) = 0.066$ it is obvious that there is a well-rounded broad anomaly extending over a large temperature range and barely perceptible in the absence of careful resolution. Heat capacities are presented in table 7.

$x(Cd) = 0.005$. A single well-defined anomaly was found in this sample. The transitional heat capacity is displayed in figure 3. Differences between the heat capacities of $Cd_{0.0005}Fe_{2.995}O_4$ and pure Fe_3O_4 are displayed in figures 4 and 5. Heat capacities can be found in table 8. Enthalpy and entropy of transition are presented in table 10.

$x(Cd) = 0.010$. A single anomaly was observed in this sample. The transitional region heat capacity is displayed in figure 3. Differences between the heat capacities of $Cd_{0.010}Fe_{2.990}O_4$ and pure Fe_3O_4 are displayed in figures 4 and 5. Heat capacities will be found in table 9. Enthalpy and entropy of transition are presented in table 10.

THERMODYNAMIC FUNCTIONS

The molar standard entropy increments and standard enthalpy increments divided by temperature are listed in table 11 at 298.15 K for selected compositions studied in this research and for Fe_3O_4 samples from the literature. More extensive tables are available.[17] All these values have been obtained by smoothing or by integration of a least-squares polynomial fit by a digital computer through the points in non-transition regions. Integration of the non-transitional heat capacity above 120 K showed a decrease in the 0.5 K entropy increments. The decrease passed through a minimum near 150 K at which point the trend reversed. This was interpreted as being indicative of a long post-transitional tail. The transitional properties of pure Fe_3O_4 were recalculated using a new "lattice" heat-capacity curve and the same relative

TABLE 11. Thermodynamic properties at 298.15 K
(cal_{th} = 4.184 J)

Sample	$\frac{S°(T)-S°(0)}{cal_{th}\ K^{-1}\ mol^{-1}}$	$\frac{\{H°(T)-H°(0)\}/T}{cal_{th}\ K^{-1}\ mol^{-1}}$
Parks and Kelley[1]	35.1	—
Millar[5]	34.69±0.2	—
Westrum and Grønvold[3]	34.93±0.05	19.91±0.04
$Zn_{0.005}Fe_{2.995}O_4$	34.80±0.05	19.82±0.04
$Zn_{0.066}Fe_{2.934}O_4$	34.81±0.05	19.76±0.04
$Cd_{0.005}Fe_{2.995}O_4$	34.95±0.05	19.86±0.04
$Cd_{0.010}Fe_{2.990}O_4$	34.78±0.05	19.76±0.04

difference of the heat capacity among the various samples in non-transition regions was maintained in the "lattice" curves thus preserving consistency. For uniformity, the "lattice" polynomials had identical powers, linear translation, and scale factor.

Below 5 K the heat capacities were extrapolated using the Debye limiting law. Since nuclear spin and isotopic mixing contributions have not been included in the entropy and derived functions, these functions are practical values for use in chemical-thermodynamic calculations.

4. Discussion

Selected transitional thermal properties have been listed in table 12. The total net transitional enthalpy ΔH_t varies slightly at low dopant levels suggesting that the energetics of the phenomena in the transition region are altered slightly even at lowest dopant levels. Significantly affected at all dopant levels, however, are the temperatures of the C_p maxima and their magnitudes, and the presence or absence of two anomalies.

TABLE 12. Selected transitional properties of $M_xFe_{3-x}O_4$ samples. Subscripts t, l, and h refer to total, lower-temperature, and higher-temperature transitions
(cal_{th} = 4.184 J)

M	—	Mn	—	Zn	Cd	?	Cd	Zn
x	0	0.008	0	0.005	0.005	?	0.010	0.066
Footnote	*a*	*b*	*c*	*d*	*d*	*e*	*d*	*d*
T_l/K	113.3	117.0	117.30	110.57	114.66	114.2	105.7	80
T_h/K	118.88	123.0	(119)	119.09	—	—	—	—
$\Delta H_t/cal_{th}\ mol^{-1}$	164	139	140	142	155	108	104	70
$\Delta H_l/cal_{th}\ mol^{-1}$	66	68	140	126	155	108	104	70
$\Delta H_h/cal_{th}\ mol^{-1}$	98	71	—	16	—	—	—	—
$\Delta S_t/cal_{th}\ K^{-1}\ mol^{-1}$	1.4	1.8	1.2	1.1	1.3	1.0	0.98	0.87
$C_{p,l}(max.)/cal_{th}\ K^{-1}\ mol^{-1}$	33.2	27.2	109.6	53.7	101.5	40.0	31.1	10.4
$C_{p,h}(max.)/cal_{th}\ K^{-1}\ mol^{-1}$	117	(46.8)	28.8	36.1	—	—	—	—

[a] Reference 3. [b] Reference 5. [c] This work: two large magnetite crystals. [d] This work. [e] Reference 2: impure magnetite.

Moreover, it is observed that the higher-temperature anomaly migrates upwards for low mole fractions of dopant ions whose radii are not significantly different from Fe^{3+}. For the larger Cd^{2+} ion, even for $x(Cd) = 0.005$, bifurcation is not observed, whereas the Zn^{2+} of comparable mole fraction shows two anomalies. The magnitude of the ΔH_t and the C_p maximum of the sample with $x(Cd) = 0.005$ shows that the two anomalies are coincident.

The magnetite crystal shows only a high-temperature shoulder. However, since two crystals were involved, superposition of two peaks, one for each sample, cannot be excluded. If such superposition is present, then on the basis of the sensitivity of the breadth and magnitude of the C_p maxima to mole fraction of dopant, the "shoulder" is due to a crystal of *lower* purity. The higher-temperature transition is raised in temperature relative to that of the other crystal and to the same transition in pure Fe_3O_4.

The quality of the doped Fe_3O_4 samples is verified by the trend of the heat capacity in non-transitional regions. Formation of two cubic phases, *e.g.* $ZnFe_2O_4$ and Fe_3O_4 for the zinc-doped, and $CdFe_2O_4$ and Fe_3O_4 for the cadmium-doped samples, would result in values of the molar non-transitional heat capacity lower than that for pure Fe_3O_4. Above 120 K the heat capacity for all other ferrites is lower than that of pure Fe_3O_4; hence, diphasic material would have a heat capacity given by the mass-adjusted arithmetical sum of the two phases. Above 120 K, the heat capacities of all doped Fe_3O_4 samples are greater than that of pure Fe_3O_4, and the difference increases with mole fraction of dopant. Hence, attribution of the two anomalies to sample inhomogeneity would be inconsistent with the results.

Since clearly both structural and electronic changes are involved in Fe_3O_4 near 120 K, it is logical to assume that the two peaks in the heat capacity are to be identified with these transformations.

HIGHER-TEMPERATURE TRANSITION

The higher-temperature transition is suspected to be electronic in nature and to represent an electronic excitation rather than the usual conduction electron contribution (characteristic of metals) to the heat capacity. Upward migration of the transition temperature with low mole fraction of dopant [$x(Mn) = 0.008$ and $x(Zn) = 0.005$] and the corresponding decrease in electron concentration is consistent with an electron lattice-gas crystallization of the Wigner-type.[21] Samara[22] observed a decrease in the transition temperature of Fe_3O_4 with increasing pressure. The observed increase in the temperature of the higher-temperature transition at low dopant levels observed in this study is entirely consistent with the results of Samara if one considers that a *slight* increase in lattice parameter due to the inclusion of the $x(Zn) = 0.005$ and $x(Mn) = 0.008$ dopants is, in effect, a "negative" pressure; hence, an *increase* in the electronic transition temperature is anticipated and found for these low mole fractions of dopant. At dopant levels in excess of $x = 0.005$, bifurcation no longer is evident and the single anomaly is suppressed and smeared-out over a temperature range which increases with increasing mole fraction of dopant.

Disappearance of the C_p maximum associated with this electronic transition at high mole fractions of dopant, does not imply elimination of the resistivity changes.

In fact, Domencali[23] found a minimum in the resistivity change of Fe_3O_4 with temperature near 350 K. The heat capacity in this region[5] showed neither markedly anomalous behavior nor even a subtle change on comparison of the Fe_3O_4 heat capacity with that of $ZnFe_2O_4$ over the same temperature region. On this basis, the expected resistivity change near 120 K will be much smaller and more gradual in highly doped samples. Our relative resistance measurements on $Zn_{0.066}Fe_{2.934}O_4$ and $Cd_{0.010}Fe_{2.990}O_4$ compared with pure Fe_3O_4 are consistent with these expectations.

The much greater influence of Cd^{2+} doping noted in table 12 on the thermal anomalies relative to that of Zn^{2+} is consistent inasmuch as Cd causes a greater lattice expansion than does Zn at an equivalent mole fraction of dopant. Here the dopant can no longer be treated as a minor perturbation on the lattice system because of the real differences in the parameters of the ions concerned. The Wigner model thus becomes inapplicable and at sufficiently high mole fractions of dopant the distortions predicted by molecular-field approximations become relevant.

THE LOWER-TEMPERATURE TRANSITION

The relative insensitivity of the low-temperature peak to impurities as well as its gradual suppression with increased impurity levels and its downward migration is consistent with ascription to a phenomenon of the more usual order-disorder type with a second-order character and its relation to a structural transition. Similar systematics occur in VO_2 and Ti_4O_7.[24,25]

These results are also totally consistent with the observations of Miyahara,[26] who found consistent decreases in the magnetization transition temperature of Al, Co, Ni, Cu, Zn, and Ti dopants at mole fractions greater than 0.05.

5. Conclusion

This study confirms the reality of the bifurcation originally observed in pure synthetic Fe_3O_4,[3] on samples prepared in different laboratories, by different techniques beyond any reasonable doubt.[27] The profiles and the ΔH_t's of the two anomalies permit us to draw tentative conclusions about the mechanism underlying the transitions.

Bifurcation is seen to be affected both by the identity and the amount of dopant. The results of this study indicate that many other measurements on Fe_3O_4 have been made on relatively impure materials. The effects occasioned by impurities have been mistakenly attributed as being those of a pure sample. Millar's[2] impurity level, for example, must approximate or exceed that of $Cd_{0.005}Fe_{2.995}O_4$ since both show a single anomaly and have nearly the same transition temperature (but the former has a smaller ΔH_t). In addition, upward migration of the higher-temperature transition with mole fraction of dopant and its ultimate disappearance suggests that it is electronic in nature and of the Wigner-type. The behavior of the lower-temperature transition and its continued presence at high mole fractions of dopant suggest that it is the structural transition from the inverse spinel to the assymetric low-temperature phase. A-site interactions have been shown to be very important in Fe_3O_4; thus, the approximation used in various theoretical considerations[28,29] of the Verwey

transition, of B-site interactions only, with only constant field A-site perturbations is an over-simplification.[30] Multiple transitions in Fe_3O_4 are consistent with recent analyses.[30–33]

We are grateful to Professor B. J. Evans for penetrating insight into crystal physics, sample preparation, and characterization, as well as the continual encouragement of this research endeavor initiated under a contract with the Division of Research of the U.S. Atomic Energy Commission and subsequently completed under funding from the National Science Foundation.

REFERENCES

1. Parks, G. S.; Kelly, K. K. *J. Phys. Chem.* **1926,** 30, 47.
2. Millar, R. W. *J. Amer. Chem. Soc.* **1929,** 51, 215.
3. Westrum, E. F., Jr.; Grønvold, F. *J. Chem. Thermodynamics* **1969,** 1, 543.
4. Bartel, J. J.; Westrum, E. F., Jr. *AIP Conf. Proc.* **1973,** 10, 1393; **1975,** 24, 86.
5. Bartel, J. J.; Westrum, E. F., Jr. *J. Chem. Thermodynamics* **1976,** 8, 575.
6. Verwey, E. J. W.; de Boer, J. H. *Rec. Trav. Chim. Pays-Bas. Belg.* **1936,** 55, 531.
7. Verwey, E. J. W.; Haaijam, P. W.; Romeyn, F. C. *J. Chem. Phys.* **1947,** 15, 174.
8. Verwey, E. J. W.; Haaijam, P. W. *Physica* **1941,** 8, 979.
9. Shannon, R. D.; Prewitt, C. T. *Acta. Cryst.* **1969,** B25, 925.
10. Evans, B. J.; Westrum, E. F., Jr. *Phys. Rev. B* **1972,** 5, 3791.
11. *Catalog of X-Ray Powder Data,* American Society for Testing Materials, No. 2–0975.
12. *Ibid.* No. 1–1109.
13. Magnetite crystals kindly loaned by Professor B. J. Evans, Department of Geology and Mineralogy, The University of Michigan, Ann Arbor, Michigan 48104, U.S.A.
14. *Photography of Powder Diffraction Patterns; Guinier Type X-Ray Focussing Camera,* Ingenjorsfirman Instrumenttjanst, Sudoyberg, Sweden, **1971.**
15. Parrish, W. *Acta Cryst.* **1960,** 13, 838.
16. Lindqvist, O.; Wegelin, F. *Ark. Kemi.* **1967,** 28, 179.
17. Detailed supplementary information on X-ray structural patterns for some samples and detailed thermodynamic functions for all samples are presented in an NAPS document No. 02766 for 17 pages of supplementary material. Order from ASIS/NAPS c/o Microfiche Publications, 440 Park Avenue South, New York, N.Y. 10016 U.S.A. Remit in advance for each NAPS accession number. Make checks payable to Microfiche Publications. Photocopies are $5.00. Microfiche are $3.00. Outside of the U.S. and Canada, postage is $2.00 for a photocopy or $1.00 for a fiche.
18. Carlson, H. G., Ph.D. thesis, the University of Michigan, Ann Arbor, Michigan, **1964** *Diss. Abstracts* **1965,** 26, 1, 111.
19. Westrum, E. F., Jr. *J. Chem. Educ.* **1962,** 39, 443.
20. Stimson, H. F. *J. Res. Nat. Bur. Stand.* **1961,** 42, 209.
21. Wigner, E. *Trans. Faraday Soc.* **1938,** 34, 678. Also Mott, N. F.; Davis, E. A. *Electronic Processes in Non-crystalline Materials.* Clarendon Press: Oxford. **1971.**
22. Samara, G. A. *Phys. Rev. Lett.* **1968,** 21, 795.
23. Domencali, C. A. *Phys. Rev.* **1950,** 78, 458.
24. Reyes, J. M.; Marks, J. R.; Sayer, M. *Solid State Communications* **1973,** 13, 1953.
25. Schlenker, C.; Lakkis, S.; Coey, J. M. D.; Marezio, M. *Phys. Rev. Lett.* **1968,** 21, 795.
26. Miyahara, Y. *J. Phys. Soc. Japan* **1972,** 32, 629.
27. *Cf.* also Buchwald, R. A.; Hirsch, A. A. *Bull. Amer. Phys. Soc.,* 1975, 20, 383; *Solid State Commun.* **1975,** 15, in the press.
28. Sokoloff, J. B. *Phys. Rev. B* **1973,** 5, 4492 and references contained therein.
29. Cullen, J. R.; Callen, E. R. *Phys. Rev. B* **1973,** 7, 397, and references therein.
30. Rajan, V. T.; Avignon, M.; Falicov, L. M. *Solid State Commun.* **1974,** 14, 149.
31. Tanaka, T.; Chen, C. C. *AIP Conf. Proc.* **1974,** 24, 89.
32. Sokoloff, J. B. *AIP Conf. Proc.* in the press.
33. Iizumi, M.; Shirane, G. *Solid State Commun.* **1975,** 17, 433.